



Characterization of dynamics and mechanism in the self-assembly of AOT reverse micelles

Cite as: J. Chem. Phys. **149**, 144901 (2018); <https://doi.org/10.1063/1.5042771>

Submitted: 04 June 2018 . Accepted: 17 September 2018 . Published Online: 11 October 2018

Ryo Urano , George A. Pantelopulos, Shanshan Song, and John E. Straub 



View Online



Export Citation



CrossMark

ARTICLES YOU MAY BE INTERESTED IN

[Statistical efficiency of methods for computing free energy of hydration](#)

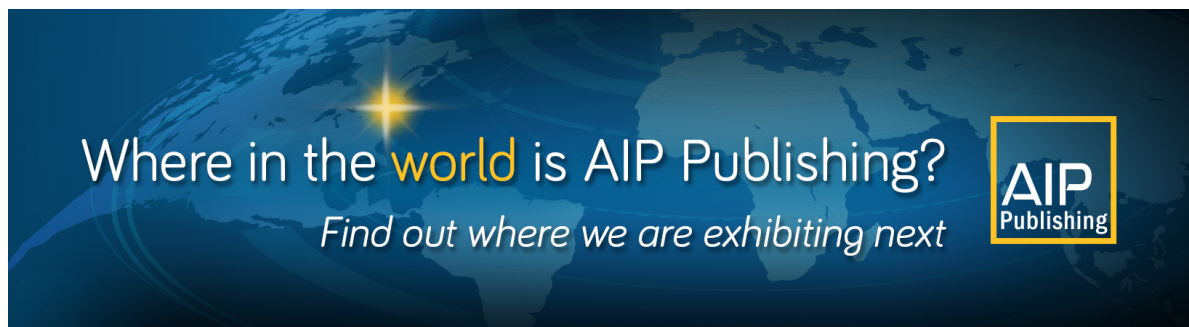
The Journal of Chemical Physics **149**, 144111 (2018); <https://doi.org/10.1063/1.5041835>

[Quantifying structural dynamic heterogeneity in a dense two-dimensional equilibrium liquid](#)

The Journal of Chemical Physics **149**, 144504 (2018); <https://doi.org/10.1063/1.5037282>

[Perspective: Crossing the Widom line in no man's land: Experiments, simulations, and the location of the liquid-liquid critical point in supercooled water](#)

The Journal of Chemical Physics **149**, 140901 (2018); <https://doi.org/10.1063/1.5046687>



Characterization of dynamics and mechanism in the self-assembly of AOT reverse micelles

Ryo Urano,^{a)} George A. Pantelopulos,^{a)} Shanshan Song, and John E. Straub^{b)}

Department of Chemistry, Boston University, 590 Commonwealth Avenue, Boston, Massachusetts 02215, USA

(Received 4 June 2018; accepted 17 September 2018; published online 11 October 2018)

Reverse micelles (RMs) are recognized as a paradigm of molecular self-assembly and used in a variety of applications, such as chemical synthesis and molecular structure refinement. Nevertheless, many fundamental properties including their equilibrium size distribution, internal structure, and mechanism of self-assembly remain poorly understood. To provide an enhanced microscopic understanding of the assembly process and resulting structural distribution, we perform multiple nonequilibrium molecular dynamics simulations of dioctyl sulfosuccinate sodium salt (AOT) RM assembly, quantifying RM size, water core structure, and dynamics. Rapid assembly of smaller RM from a random mixture is observed to establish a constant AOT water loading within a nanosecond consistent with a diffusion-adsorption mechanism validated through the Monte-Carlo simulation of a model system. The structure of RM water cores and RM molecular volume during RM assembly is characterized during the AOT assembly process. A moment-closure equation is developed from a novel master equation model to elucidate the elementary events underlying the AOT self-assembly process. The resulting kinetic model is used to explore the role of monomer addition and dissociation, RM association and dissociation, and RM collision-induced exchange, all dependent on average RM size, which provides fundamental insight regarding the mechanisms and time scales for AOT RM self-assembly. The nascent dynamics that rapidly establish water loading, intermediate time scales of RM fusion, and longer time scale dynamics of inter-RM exchange essential in establishing the equilibrium condition are quantified through these kinetic models. Overall, this work provides insight into AOT RM self-assembly and provides a general theoretical framework for the analysis of the molecular self-assembly dynamics and mechanism. *Published by AIP Publishing.* <https://doi.org/10.1063/1.5042771>

INTRODUCTION

Reverse micelles (RMs), formed in the environments of water, amphiphilic surfactant, and rich hydrophobic solvent, are utilized in applications such as chemical synthesis,¹ drug delivery systems,^{2–4} investigation of membrane protein transport,⁵ and solute encapsulation.^{6,7} Dioctyl sulfosuccinate sodium salt (AOT) is perhaps the most widely studied RM surfactant, as AOT RMs form without co-surfactant molecules, simplifying the phase diagram for these mixtures.

Water stabilizes the association of surfactants in the presence of the hydrophobic solvent, enabling the formation of large RMs.⁸ Several experiments have shown that the number of waters solvating surfactant molecules within RMs is directly dependent on the water loading of the system.^{9–14} AOT and water form a stable structural network in moderately low water loadings through AOT-water pair formation.^{8,15–17} The dynamics of the water core in RMs are of significant interest due to the observed dynamical heterogeneity of water reorientation, and several studies have explored the behavior of water as a function of distance from surfactant head regions.^{9,18–22}

The effect of AOT-water interaction on the water structure has been studied via spectroscopic^{8,10,11,23} and NMR¹⁴ experiments. Jain *et al.* classified water structures into surface bound, trapped, and free states and found the maximum hydration number of AOT molecules to be 12.¹¹ In an NMR study by Hauser *et al.*,¹⁴ each AOT was found to influence the behavior of up to 13 water molecules, with two water adopting a strongly bound complex with AOT. Photon correlation experiments⁸ have shown hydrogen bond interactions as a dominant energetic contribution in RM formation. Additionally, free energy models quantifying the difference between free AOT and RM states have been proposed in order to characterize the key thermodynamic driving forces in the AOT RM assembly.^{24–26}

Exchange of RM components upon the collision of RMs plays a major role in the RM assembly and dynamics of equilibrium. The percolation of electric conductance and its dependence on temperature or volume fraction of RMs^{27–33} have been used to measure the effect of collision-induced exchange on RM dynamics as conductance is strongly influenced by inter-RM interactions. This exchange process is related to mass transfer among RMs and is of importance to applications using RM encapsulation. In addition to collisions, RMs also undergo coalescence into larger RMs. The time scale of intermicelle exchange and coalescence has been measured at equi-

^{a)}R. Urano and G. A. Pantelopulos contributed equally to this work.

^{b)}Electronic mail: straub@bu.edu

librium, where AOT and water exchange rates were found to be 10^2 – 10^3 times faster than coalescence.³⁴ The exchange rate (k_{ex}) has been observed to depend on the mixture composition, temperature, and presence of salt and was measured to be 10^7 M⁻¹ s⁻¹ at 25 °C with 0.2M AOT, under the same conditions as the aforementioned measurements.^{35–38}

Robinson *et al.* measured k_{ex} at various concentrations, temperatures, chain lengths of the alkane solvent, and additives using stopped flow experiments.³⁴ As the temperature increased and hydrophobic solvent chain lengthened, RM sizes were found to become smaller. As AOT concentration increased, k_{ex} increased by several orders of magnitude. Addition of co-surfactant molecules such as toluene, benzyl alcohol, and cholesterol impacted k_{ex} as well. By adding benzyl alcohol as a co-surfactant, k_{ex} increased by a factor of up to 20. The estimated exchange rate constant, 10^{6-9} M⁻¹ s⁻¹, under various conditions of temperature and AOT concentration, is two to four orders of magnitude slower than predictions from free diffusion theory implying a free energy barrier to collision-induced RM fusion. In comparison to other RM-forming surfactants, such as cetyl trimethylammonium bromide (CTAB)/water/heptane chloroform mixtures, AOT RMs have a slower exchange rate and are more kinetically stable. Importantly, if k_{ex} is fast enough, bicontinuous structures beyond the RM phase are observed. As such, the RM exchange rate is critical to the stability of the RM phase.

Over the past two decades, there have been many molecular simulation studies involving RMs. Due to the utility of RM-encapsulation for the experimental measurement of protein structure, the structure of RM-encapsulated protein systems has been studied in substantial detail using molecular simulation. Tian and Garcia explored the dynamics and location of proteins in RMs³⁹ and the effect of RMs on the ubiquitin structure and dynamics.⁴⁰ Straub and co-workers explored the effect of charged and zwitterionic termini on a RM-spanning protein on the structure and dynamics of RMs⁴¹ as well as the effect of RM-encapsulation on amyloidogenic peptide aggregation.⁴² Eskici and Axelsen also investigated the role of RM-encapsulation on the structure of amyloid beta.⁴³

Molecular simulation has also been used to study the microscopic mechanism of self-assembly and the dynamics of water within RM systems.^{44–46} In seminal studies by Ladanyi *et al.*, it was shown that the RM water core dynamics is dependent on distance from the surfactant head molecule and water loading,^{47–50} providing an explanation of water loading dependence of water dynamics within RMs.^{51,52} Eskici and Axelsen recently estimated the size distribution of AOT RMs at a water loading of 7.5 via conventional molecular dynamics (MD) simulations⁵³ and investigated the water exchange mechanism upon the fusion of RMs.⁵⁴ Additionally, coarse-grained simulations of RM formation have demonstrated the role of the water core in the RM formation mechanism.⁵⁵

While the simulation literature has focused on the dynamics of water and the morphology of RMs at equilibrium, the structure of RMs during self-assembly is less well understood. Nevertheless, studies have provided insight into various local structural parameters of water, such as the orientational tetrahedral order, translational tetrahedral order, local structure

index (LSI), and local density.^{56–60} Additionally, thermodynamic models of micelle formation have inspired the models of other aggregation processes, such as the assembly of clathrin baskets.⁶¹

Most AOT simulation studies have been performed from the spherical initial configurations of AOT and water molecules. For the formation of a single RM, Graeve *et al.*^{62,63} performed united atom simulations of AOT and water in an isooctane solvent initiated from random mixtures over 500 ns, leading to stable fluctuations in RM size and shape. Recently, Marchi and Abel⁶⁴ performed 1 μ s AOT self-assembly simulations in which multiple RMs were formed at a water loading of five. They observed the same number of RMs formed in each simulation and calculated the time scale of initial RM formation to be approximately 20 ns. These RMs converged to the same ellipsoidal shape observed in the past simulations of isolated RMs, validating the results of prior work. These simulations also observed the formation of transient RM collisions on the near-microsecond time scale. However, the microscopic mechanism of RM formation underlying the observed aggregation dynamics was not examined.

Three different RM self-assembly mechanisms have been proposed: a phase-separation model, a multiple-equilibrium model, and a mass action model.^{65,66} While these models describe critical concentrations, co-operative features, and size-limiting distributions of RMs, they fail to describe molecular interactions among RMs. To describe inter-RM interactions, an alternative model employing a generalized chemical master equation^{67,68} for the self-assembly process is expected to be of greater utility. In the past, master equation models were developed to describe the formation of micelles.^{69,70} Recently, Knowles *et al.*^{71–75} proposed a chemical master equation in which the analytical solutions of moments were used to model the polymerization of the amyloid- β protein. The theory employed size-independent rate constants determined from experimental results. The extension of their model to the case of RM self-assembly may provide an improved model of the RM assembly process and facilitate the identification of rates of elementary microscopic processes underlying RM assembly.

In this study, we performed multiple replicate MD simulations of AOT self-assembly in atomistic detail. Our dynamical simulations were used to develop a diffusion-adsorption (DA) model in order to elucidate the nascent association dynamics that establish RM water loading. We further developed a novel master equation model to explain the RM fusion process.

Time series of RM growth including the production of RMs, free molecule depletion, and establishment of water loading on AOT are presented. Order parameters of water within RMs offer a physical explanation for why RMs grow beyond their initial sizes after RM solvation, a time scale associated with RM fusion. A novel master equation approach is used to describe the inter-RM exchange process. By fitting the time series of RM average sizes, we obtain the kinetic rate constants of various elementary processes involved in the RM exchange mechanism. The rate constants describe how the average size of RMs is influenced by the kinetics of

these processes. The results of our study suggest that inter-RM exchange is critical in determining average RM size. This is qualitatively different from the kinetics of normal surfactant formation which can be explained without inter-micelle interaction. This work provides critical insight into the microscopic structure of AOT RMs during self-assembly, the interplay of the RM molecular structure and size, and a new formalism for the analysis of RM self-assembly kinetics.

METHODS

Water order parameters

The following order parameters were used to characterize the structure of water molecules during RM water core formation. Each parameter assesses unique aspects of the RM-encapsulated-water structure.⁵⁶

Orientational tetrahedral order

For the nearest neighbor water oxygen atoms, the order parameter Q defined as

$$Q = 1 - \frac{3}{8} \sum_{j=1}^3 \sum_{k=j+1}^4 \left(\cos \Psi_{jk} + \frac{1}{3} \right)^2 \quad (1)$$

provides a measure of orientational tetrahedral order.^{57,58} Ψ_{jk} is the angle formed by a selected oxygen j and its nearest neighbor oxygen atoms k . $Q = 0$ when bond-orientation is similar to an ideal gas and $Q = 1$ when the structure is a regular tetrahedron.

Translational tetrahedral order

Translational tetrahedral order,⁵⁸ S_k , is defined as

$$S_k = 1 - \frac{1}{3} \sum_{k=1}^4 \frac{(r_k - \bar{r})^2}{4\bar{r}^2}, \quad (2)$$

where r_k is the distance from the selected oxygen to the nearest neighbor oxygen, k , and \bar{r} is the arithmetic mean of the four nearest neighbor water oxygens. $S_k = 1$ for a perfect tetrahedron.

Local structure index

The local structure index,⁵⁹ LSI, quantifies the gap between the first and second hydration shell of water defined as

$$\text{LSI} = \frac{1}{n} \sum_{i=1}^n (\Delta(i) - \bar{\Delta})^2, \quad (3)$$

where oxygen-oxygen distances are ordered as $r_1 < r_2 < \dots < r_n < 3.7 \text{ \AA} < r_{n+1}$, $\Delta(i) = r_{i+1} - r_i$, and $\bar{\Delta}$ is the average of $\Delta(i)$.

Local density

The local density has various definitions.^{56,76} We employ the measure used by Duboue-Dijon and Laage,⁵⁶

$$\rho = \frac{1}{V}, \quad (4)$$

where V is calculated through the Voronoi tessellation of heavy atoms.⁵⁶ An example of the Voronoi tessellation for a single RM is shown in Fig. S1 of the [supplementary material](#).

Steinhardt-Nelson order parameters

Steinhardt-Nelson bond orientational order parameters⁷⁷⁻⁷⁹ are often used to distinguish crystal structures in molecular simulations. The order parameter is calculated from the local environment around a particle without any reference frame.

The complex vector $q_{lm}(i)$ of particle i in the $(2l + 1)$ dimensional complex vector is defined as

$$q_{lm}(i) = \frac{1}{N_b(i)} \sum_{j=1}^{N_b(i)} Y_{lm}(r_{ij}), \quad (5)$$

where $N_b(i)$ is the number of the nearest neighbors of particle i , $Y_{lm}(r_{ij})$ are the spherical harmonics, and r_{ij} is the vector from particle i to particle j . Neighbors are defined as all particles that are within a given cutoff r_c around a central particle. To make the order parameters invariant with respect to the rotation of the reference frame, the rotationally invariant local bond parameters are defined as

$$q_l(i) = \left(\frac{4\pi}{2l+1} \sum_{m=-l}^l |q_{lm}(i)|^2 \right)^{1/2} \quad (6)$$

and the third-order invariant is defined as

$$w_l(i) = \sum_{m_1+m_2+m_3=0} \begin{pmatrix} l & l & l \\ m_1 & m_2 & m_3 \end{pmatrix} q_{lm_1}(i) q_{lm_2}(i) q_{lm_3}(i), \quad (7)$$

where the coefficients (\dots) are the Wigner $3j$ symbols. We use the normalized quantity

$$\bar{w}_l \equiv \frac{w_l}{\left(\sum_{m=-l}^l |q_{lm}|^2 \right)^{3/2}}. \quad (8)$$

We evaluate the case of $l = 6$ symmetry for $q_b(i)$ and \bar{w}_b which should both be near zero for liquid or gas-like structures. By abandoning the phase information on the spherical harmonics, a rotationally invariant bond-orientational order parameter may be also obtained. To measure the correlation in bond-orientational order between neighboring water molecules, we measure the average dot product of q_6 of all waters with their nearest neighbors, previously employed by Auer and Frenkel.⁸⁰

Hierarchical clustering of AOT and water

To identify aggregates of AOT and water, a single-link hierarchical clustering method was used to identify the clusters of AOT sulfur atoms and water oxygens based on Cartesian coordinates with a cut-off distance of 1.0 nm. There is some variation in the numbers of water and AOT composing aggregates due to fluctuations beyond this cutoff. This distance was selected as the most well-behaved and consistent via visual inspection.

Distribution shape parameter fitting

We quantified the distributions of AOT and water in RMs derived from MD and compared those profiles with the

results of stochastic diffusion-adsorption simulations. These distributions were computed and fit to gamma distributions using packages and libraries in R.^{81–88} The gamma distribution is defined as

$$f(x) = \frac{1}{s^a \Gamma(a)} x^{(a-1)} \exp\left(-\frac{x}{s}\right), \quad (9)$$

where $x \geq 0$, the shape parameter $a > 0$, and the rate parameter $s > 0$.

Monte-Carlo diffusion-adsorption model

To serve as a standard reference for random diffusion-adsorption kinetics in RM solvation assembly, we developed a Monte-Carlo (MD) diffusion-adsorption simulation model. Within the model, water may adsorb to water, water may adsorb to AOT, and AOT may adsorb to AOT. AOT and water are represented as spherical points undergoing random diffusion in Cartesian coordinates simulated using cubic periodic boundary conditions with 15-nm edges in each dimension. A 1 nm encounter radius was used for all adsorption interactions, the same as the hierarchical clustering cutoff used for RM identification. Ten diffusion-adsorption simulations were initiated from the same 10 initial conditions as the RM self-assembly MD simulations. MC displacements (each taken in a random direction) were converted into time steps of 1 ps based on the diffusion coefficients of AOT and water and the displacement size. The displacement size per step was taken to be at least an order of magnitude smaller than the encounter radius. Each simulation was 50 ns long.

Diffusion coefficients of monomeric AOT measured from MD simulations and water in the isooctane solvent were used to determine MC displacement magnitudes. The same initial conditions for the equilibration of MD trajectories of AOT self-assembly were used to perform the RM assembly simulations. The monomer diffusion coefficient was found to be 21.9 nm² ns⁻¹ for water and 0.37 nm² ns⁻¹ for AOT. Upon encountering another molecule, either (1) water-water adsorption occurs with the mass of the adsorbed water transferred to the other water, effectively forming a water “cluster,” while the adsorbed water is removed from the system;

(2) water-AOT adsorption occurs, in which the mass of water is transferred to the AOT, and the adsorbed water is removed from the system; or (3) AOT-AOT adsorption occurs, in which the mass of the adsorbed AOT is transferred to the other AOT, and the adsorbed AOT is removed from the system. Increases in mass decrease the displacement of an AOT or water particle in a way that conserves the magnitude of the momentum. The isooctane solvent is treated implicitly in these simulations.

Extension of master equation for aggregation

To model the amyloid- β aggregation mechanism, Knowles *et al.*^{71,72,74} developed a kinetic master equation model capable of describing a nucleation-polymerization mechanism. The model includes elementary processes including rates of monomer association, dissociation, oligomer fusion, fragmentation, and nucleation, accounting for anticipated primary nucleation pathways. They obtained an analytical solution for polymer number concentration and polymer mass concentration. The average aggregate size works well as this primary parameter and is simple to measure via both experiment and simulation. Via their analytical solution and numerical simulations, Michaels and Knowles successfully reproduced experimentally measured data of amyloid- β aggregation, elucidating the microscopic mechanism of amyloid fibril formation in a number of systems.⁷⁵

We extend the model of Knowles and co-workers to study the AOT self-assembly process. (1) We obtain rate constants for the AOT aggregation processes from simulation data that may be directly related to experiment. (2) We generalized the Knowles model by introducing collision-induced molecular exchange, an important part of the RM equilibration process that occurs when RMs collide, thus playing a major role in mass transfer in RM-encapsulated molecules. Upon introduction of a molecular exchange process for the generalized model, it is possible to identify a unique solution in parameter space. A schematic view of each process is shown in Fig. 1.

The master equation for the dependence of the aggregate concentration, $f(t, j)$, of aggregate size j at time, t , is

$$\begin{aligned} \frac{\partial f(t, j)}{\partial t} = & 2k_+ m(t) f(t, j-1) f(t, j-1) - 2k_+ m(t) f(t, j) + 2k f(t, j+1) - 2k f(t, j) - \bar{k}_-(j-1) f(t, j) + 2\bar{k}_- \sum_{i=j+1}^{\infty} f(t, i) \\ & + \bar{k}_+ \sum_{k+l=j} f(t, k) f(t, l) - 2\bar{k}_+ f(t, j) \sum_{i=2}^{\infty} f(t, i) + k_n m(t)^2 \delta_{j,2} + k_{ex} \sum_{m=2}^{\infty} \sum_{k=1}^{m-1} \sum_{l+k=j} f(t, j) f(t, m-k) \\ & + k_{ex} \sum_{l=k+1}^{\infty} \sum_{k=1}^{l-k=j} \sum_{m=2}^{\infty} f(t, j) f(t, m+k) - k_{ex} f(t, j) (j-1) \sum_{i=2}^{\infty} f(t, i) - k_{ex} f(t, j) \sum_{i=2}^{\infty} f(t, i) (i-1), \end{aligned} \quad (10)$$

where $m(t)$ is monomer concentration at time t and the initial nucleus size is 2. The first nine terms are the same as in the model of Knowles and co-workers, including the aggregation process of monomer addition, k_+ , $(j-1, 1) \Rightarrow (j)$, and $(j, 1) \Rightarrow (j+1)$; the dissociation process of monomer from an aggregate, k_- , $(j+1, -1) \Rightarrow (j)$, and $(j, -1) \Rightarrow (j-1)$; the fragmentation

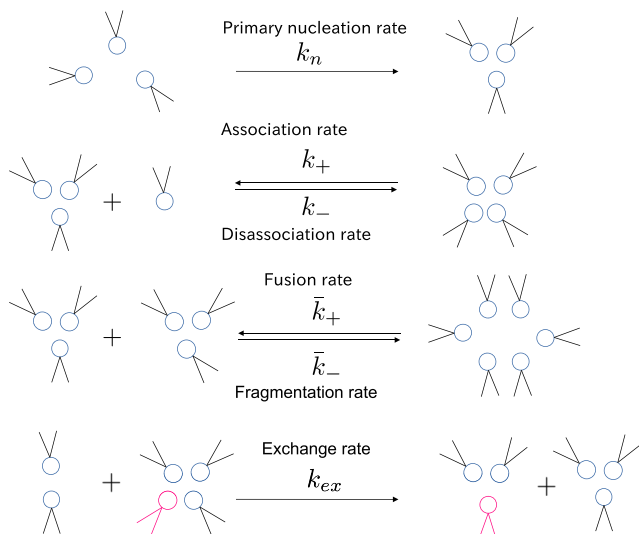


FIG. 1. Schematic view of each elementary microscopic process modeled using the generalized master equation approach, including nucleation, association, disassociation, fusion, fragmentation, and collision-induced exchange.

process of oligomers, \bar{k}_- , $(j) \Rightarrow (j - i, i)$ for $(i < j)$, $(i) \Rightarrow (j, i - j)$ for $(i > j)$; the fusion process of oligomers, \bar{k}_+ , $(k, l) \Rightarrow (j)$, and $(j, i) \Rightarrow (j + i)$ for $(i > 2)$; and the primary nucleation process, k_n (nuclei size, $n_c = 2$) $(1, 1) \Rightarrow (2)$.

The last four terms add a collision induced exchange process with a characteristic rate constant, k_{ex} . This novel extension of the model of Knowles and co-workers captures elementary rate process control to the kinetics of surfactant

assembly. The first two exchange terms represent the increase of size j through absorption $(l, m) \Rightarrow (j = l + k, m - k)$ for $l < j$ and emission $(l, m) \Rightarrow (j = l - k, m + k)$ for $l > j$, respectively. The last two terms capture decrease in aggregate size j due to molecular absorption and emission.

The first two moments of the distribution and average size are defined as

$$P(t) = \sum_{i=2}^{\infty} f(t, i), \quad (11)$$

$$M(t) = \sum_{i=2}^{\infty} i \times f(t, i), \quad (12)$$

$$N(t) = \frac{M(t)}{P(t)}, \quad (13)$$

where $P(t)$ is the aggregate number concentration, $M(t)$ is the aggregate mass concentration, and $N(t)$ is the average aggregate size. In this extended model, by performing the summation from $j = 2$ to infinity, we can obtain closed moment equations for aggregate concentration and mass concentration,

$$\frac{dP}{dt} = -\bar{k}_+ P^2(t) - k_{ex} P^2(t) + \bar{k}_- [M(t) - 3P(t)] + k_n m(t)^2, \quad (14)$$

$$\frac{dM}{dt} = 2 \left[m(t) k_+ - k_- - \bar{k}_- - k_{ex} P(t) \right] P(t) + 2k_n m(t)^2, \quad (15)$$

where we use the following transformation for exchange reactions resulting in the aggregates of size j by association $(l, m) \rightarrow (j = l + k, m - k)$ and dissociation $(l, m) \rightarrow (j = l - k, m + k)$,

$$\sum_{j=2}^{\infty} \sum_{m=2}^{\infty} \sum_{k=1}^{m-1} \sum_{l+k=j} f(t, j) f(t, m - k) + \sum_{j=2}^{\infty} \sum_{l=k+1}^{\infty} \sum_{k=1}^{l-k=j} \sum_{m=1}^{\infty} f(t, j) f(t, m + k) = \sum_{j=2}^{\infty} f(j) \sum_{i=2}^{\infty} (i - 1) f(i) + \sum_{j=2}^{\infty} f(j) (j - 2) \sum_{m=2}^{\infty} f(m), \quad (16)$$

$$\sum_{j=2}^{\infty} j \sum_{m=2}^{\infty} \sum_{k=1}^{m-1} \sum_{l+k=j} f(t, j) f(t, m - k) + \sum_{j=2}^{\infty} j \sum_{l=k+1}^{\infty} \sum_{k=1}^{l-k=j} \sum_{m=1}^{\infty} f(t, j) f(t, m + k) = \sum_{j=2}^{\infty} f(j) \sum_{i=2}^{j-1} i \sum_{m=2}^{\infty} f(m) + \sum_{j=2}^{\infty} f(j) \sum_{m=2}^{\infty} \sum_{i=j+1}^{\infty} i f(m). \quad (17)$$

Note that monomer size $j = 1$ is not considered as a reactant in these processes. The proportionality of k_{ex} to the squared polymer number concentration as $k_{ex} P^2(t)$ is consistent with physical intuition, as the exchange processes must occur in the presence of other RMs.

An approximate steady state solution and analytical solution for early time behavior are shown in the [supplementary material](#). The model of Knowles and co-workers⁷⁵ is recovered for $k_{ex} = 0$. The analytical solution also shows how the collision-induced exchange process affects the mean RM size observed when the early time solution is solved with $k_{+m}(0) \gg \bar{k}_-$.

System setup

The RM system was composed of 140 AOT, 700 water, and 9912 isoctane molecules, totaling 269 052 atoms, and

consistent with an overall water loading of five and expected to form RMs based on the phase diagram for this system composition.⁸⁹ The system employed cubic periodic boundary conditions, with edges of approximately 15.0 nm. AOT and isoctane were parameterized using the model developed by Abel *et al.*^{15,44} while the remainder of the system was parameterized using the CHARMM27 force field.^{90,91} The systems were constructed with the random spatial placement of all molecules in the substrate. This random spatial placement emulates the gradual injection of surfactant molecules to solution employed in experiments to investigate RM formation as a function of concentration, for which the early time scales feature a monodisperse solution of surfactants in solution.

To prepare each system, 216 isoctane molecules were pre-equilibrated in a 3.9-nm solvent box, consistent with a density of 690.95 kg/m³, equal to the experimental density.⁹² This system was copied to form a cubic box with 14.0-nm edges.

AOT and water molecules were randomly inserted into the isooctane solvent box and energy minimized to form 10 unique initial positions. The configuration of each system was then refined using the steepest descent energy minimization. All simulations were performed using the Groningen Machine for Chemical Simulations (GROMACS) simulation suite version 5.1.^{93–95}

To obtain the correct average temperature, a 100 ps NVT simulation was performed with the Bussi velocity-rescale thermostat at 298.15 K. To stabilize the system density, a 100 ps NPT simulation was conducted with the Bussi velocity-rescale thermostat at 298.15 K and the isotropic Parrinello-Rahman barostat at 1 bar and compressibility $9.0 \times 10^{-5} \text{ bar}^{-1}$. Both thermo- and barostats used a coupling time of 2 ps. All MD integration was performed using the leap-frog integrator with a 2 fs time step, constraining all bonds using linear constraint solver (LINCS).^{96,97} The LJ interactions were truncated using a switching function over a distance from 0.8 to 1.2 nm. Particle mesh Ewald (PME) was used to model electrostatics with a 1.2-nm cutoff.⁹⁸ Ten production run simulations were completed, each from a unique set of initial coordinates. Nine of the ten replicates achieved 400 ns of sampling, with one achieving 1163 ns. These production simulations employed the Nose-Hoover thermostat and Parrinello-Rahman barostat at 295.15 K and 1 bar and compressibility of $9.0 \times 10^{-5} \text{ bar}^{-1}$, respectively. Each MD simulation was performed using 10 2.6 GHz Intel XeonE5-2670s with 160 MPI threads at an overall rate of 16 ns/day.

RESULTS

Simulation results

The number of distinct clusters containing AOT observed in ten nonequilibrium MD simulations of AOT self-assembly over 400 ns is shown in Fig. 2(a). By the end of 10 400ns trajectories, we observed there to be 3–7 RMs in each system and 5 RMs on average. It is in this time scale that RM coalescence occurs. The relaxation time of RM formation has previously been calculated using the function

$$G(t) = \frac{N_{RM}(t) - N_{RM}(\infty)}{N_{RM}(0) - N_{RM}(\infty)}, \quad (18)$$

where $N_{RM}(\infty)$ is set to four and the stretched exponential,

$$\phi(t) = \exp\left(-\left(\frac{t}{\tau}\right)^\alpha\right), \quad (19)$$

was fit to each trajectory. The obtained average relaxation times,

$$\langle t \rangle = \frac{\tau}{\alpha} \Gamma\left(\frac{1}{\alpha}\right), \quad (20)$$

per trajectory are 25.6, 14.4, 12.6, 9.9, 17.0, 18.2, 16.7, 19.5, 15.7, and 21.8 ns, which are comparable with the previously reported values of 16.7, 21.7, and 24.0 ns.⁶⁴

The depletion of isolated water and AOT molecules is examined in Figs. 2(b) and 2(c). Isolated AOTs were completely depleted in the first 20 ns, and waters were depleted in just a few ns, and only 1–3 water molecules remain isolated throughout each trajectory. The solvation of AOT molecules by water is quantified by the water loading, w_0 , defined by

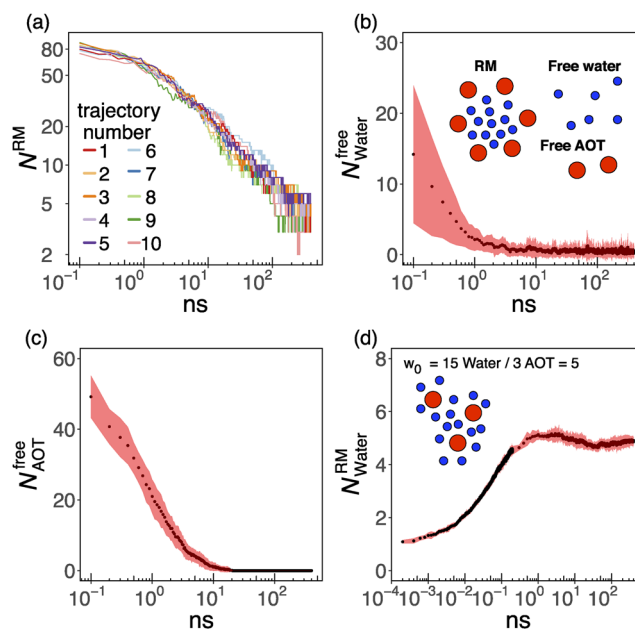


FIG. 2. (a) Logarithm of the average number of AOT clusters versus the logarithm of time for 10 AOT self-assembly trajectories. The average number of (b) free waters and (c) free AOTs over 10 trajectories. (d) Average water loading in formed RM over 10 trajectories. The red shading represents the standard deviation about the mean value shown in brown calculated from 10 trajectories as a function of time.

$w_0 = \frac{N_{Water}}{N_{AOT}}$. The water loading of the system at $N_{AOT} = 140$ and $N_{Water} = 700$ was five. Figure 2 shows the average water loading of formed RMs in all trajectories, which achieved a converged value after approximately 1 ns. These results suggest that the initial stage of RM formation consists of a process in which water molecules rapidly solvate AOT head groups to form small RMs, after which RM fusion allows the system to relax to equilibrium.

This formation mechanism is supported by the time evolution of the average number of water molecules in RM aggregates (Fig. S2 of the [supplementary material](#)). Initially, there is little fluctuation in the average number of waters per RM as the water loading relaxes to a constant value. At later times, fluctuations in the average number of water molecules per RM occur due to the coexistence of RMs of various sizes. The equilibration of the number of water molecules per RM is expected to coincide with the equilibration of the system, which should occur after 500 ns, the time scale on which water transport between RMs upon collision is reported to occur.⁶⁴

AOT solvation process

At short times, water and AOT rapidly associated to form small RMs. This process is characterized by the rapid decrease in the number of “free” water and AOT in the system over time. Free waters were depleted within 1 ns, and free AOT molecules were depleted within 20 ns. During the depletion of free water and AOT, the average water loading of AOTs rapidly converged to 5, the water loading expected from the overall H₂O:AOT ratio of the system. This rapid convergence in the AOT water loading is striking and does not appear to have been identified in previous simulations of AOT self-assembly.⁶⁴ This initial

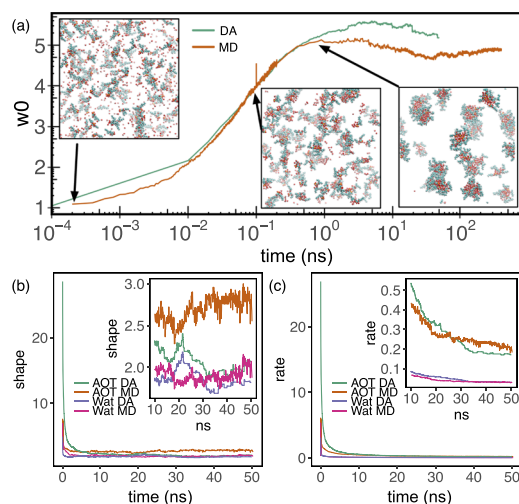


FIG. 3. (a) Average water loading over 10 trajectories derived from MD simulations (MD) and the diffusion adsorption model (DA). Inset figures are typical snapshots of the early randomized state (left) and RM solvated state (right). (b) Shape and (c) rate parameters for the gamma distribution in Eq. (9) obtained by fitting to the size distribution of AOT and water in MD simulation trajectories and DA model trajectories. Inset figures emphasize the fluctuations in the longer time scale dynamics.

RM formation process is distinct in the time scale and mechanism from the RM exchange process that occurs after 20 ns once free AOTs have been depleted and initial RM formation is apparently complete.

To explain the observation that the mean AOT water loading rapidly converges to a constant value equal to the water loading of the system, we compared our molecular simulation results with the results of a diffusion-adsorption (DA) simulation model (see Sec. II for details). In both MD and DA simulations, the average water loading per AOT was found to rapidly converge within 1 ns (Fig. 3).

The DA model does not include repulsive or attractive interactions. As such, it is important to validate whether distributions of AOT and water per cluster within the DA model are similar to those observed in the early time scale MD simulations. We fit gamma distributions of AOT and water per cluster observed at each point in time over 10 replicate DA and MD

simulations. Each fitting results in shape and rate parameters. The time series of these distributions for the DA and MD simulations appear to be well correlated with the exception of the shape of distributions for the number of AOT per cluster, for which the DA simulations are more widely distributed (Fig. 3). We evaluated the significance of the correlation between the time series of these DA and MD simulations of AOT and water cluster size via the Kolmogorov-Smirnov test, Wilcoxon signed rank test, and Wald-Wolfowitz run test. We find them to be nearly significant, with p-values between 0.1 and 0.05 (see the [supplementary material](#)). We conclude that a simple diffusion-adsorption mechanism explains the initial formation of RMs up to 20 ns, prior to the onset of RM exchange kinetics within the system.

Structural properties of RMs

The distributions of numbers of AOT and water per cluster in 0-5, 20-25, 100-105, 200-205, 300-305, and 395-400 ns are visualized in Fig. 4. Before 20 ns, less than 10 AOTs per RM are observed. Beyond 20 ns, the distribution of numbers of water and AOT per RM gradually widens. By 400 ns, the RM size distribution is broad, implying that the system has not reached equilibrium. More simulation time is necessary to reach thermodynamic equilibrium through microscopic processes (such as the exchange of surfactant and water between RMs). Distributions of the number of AOT per RM over time are shown in Fig. 5. From 0 to 1 ns, the number of AOTs per RM is exponentially distributed, suggesting that the aggregation process on this time scale results from random associations of AOT. By 10 ns, the distribution of AOTs per RM becomes well described by a gamma distribution. By 400 ns, some deviations from gamma distributions are formed as transient observations of large RMs are observed due to RM collisions, indicating the limit of our sampling.

The RM water bond-orientational order is shown in Figs. 6(a) and 6(b) at various times. Water bond-orientations are observed to evolve from the early-time value of q_6 , indicating the enhanced 6- or 12-fold coordination of waters within RMs. However, w_6 remains near-zero indicating

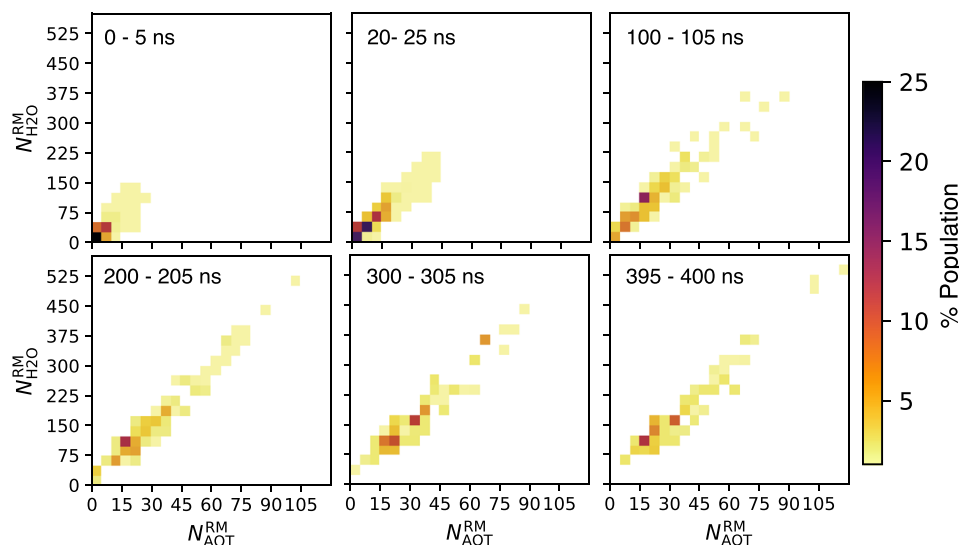


FIG. 4. Aggregate size distributions sampled from various windows in time over 10 trajectories.

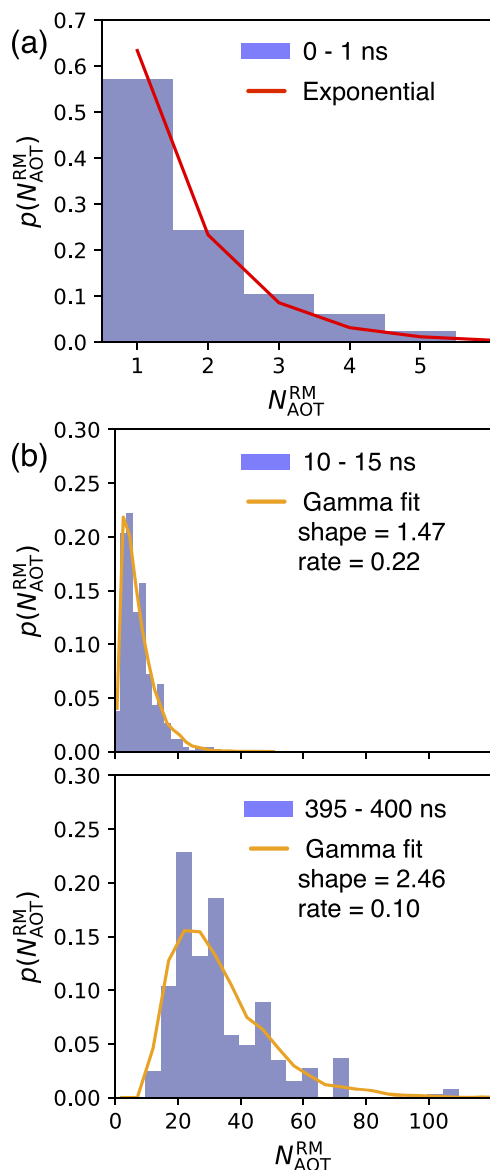


FIG. 5. Average probability distributions for the number of AOT molecules over 10 trajectories in (a) 0-1 ns and an exponential distribution and (b) 10-15 ns and 395-400 ns fit with a gamma distribution.

the orientationally disordered structural characteristics of a liquid state.

The presence of 6 and 12-fold orientational order is confirmed by the correlation function of q_6 in Fourier space. At 0.1 ns, in Fig. 6(c), the angular correlation is similar to liquid bulk water and evolves to larger values at later time. This

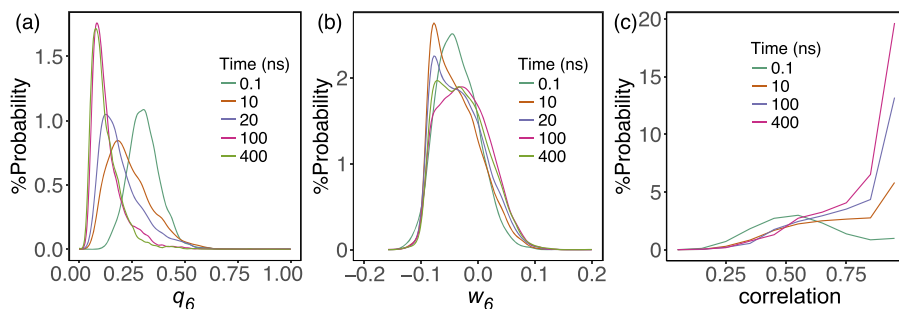


FIG. 6. Average values of Steinhardt-Nelson order parameters with index 6 for all water molecules among RMs for all trajectories in (a) q_6 (left) and (b) w_6 and (c) angular correlation of the nearest neighbor q_6 in Fourier space.

suggests that the bond orientational order of water molecules in RMs is influenced by RM size. Such deviations in the angular orientation of water in RM cores compared with bulk water have previously been observed in spatial pair correlation functions.^{47,48}

Previous simulations reported that the bond angle correlation function of waters in RMs is significantly different from that of bulk water.^{47,52} Our results suggest that RM waters have ideal gas-like tetrahedral order during the early time scale of self-assembly. Moreover, the tetrahedral order parameter does not display a clear trend as a function of RM size (Fig. 7).

We also investigated the change in molecular volume during self-assembly using Voronoi tessellations, shown in Fig. 8. We observe that water and AOT head group regions rapidly decrease in volume over the first 20 ns, during the rapid formation of small RMs, prior to a more gradual decrease during RM fusion between 20 and 100 ns, corresponding to the time scale when there are more than 8 RMs present in the system. From 150 ns and beyond the volume of RM molecules appear to have reached a steady state. This observation suggests that the further fusion of RMs does not result from a need to relax the structures of individual RM aggregates. Rather, it appears to occur due to an alternative driving force such as the reduction in surface curvature, which has classically been used to explain the narrow polydispersity in micelle sizes.

RM collision-induced exchange kinetics described via a master equation approach

The complicated time series representing the RM size and structure demonstrate RM formation on the sub-microsecond scale. We identify a RM size by the number of AOTs in a RM, also known as the aggregate number (N_{AOT}^{RM}), as the water loading of RMs fluctuates about a constant value of 5 and as can be observed in Fig. 4. The width of the sampled N_{AOT}^{RM} distributions suggests that an equilibrium structural ensemble has not been reached in these simulations, which we should expect to be monodisperse at equilibrium. As reported by Marchi and Abel,⁶⁴ the molecular transport process among RMs through RM collision is expected to play an important role on the super- μ s time scale. We employed estimated kinetic rate constants for elementary processes of association, dissociation, fusion, fragmentation, and exchange described in Fig. 1 in an extended master equation model in order to capture such long-time behavior, particularly for the characterization of average RM size.

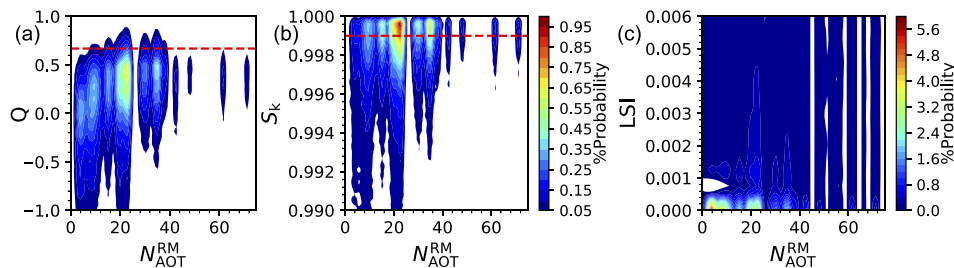


FIG. 7. Order parameters of water molecules in any RM as a function of the aggregate number of AOT: (a) orientational tetrahedral order, (b) translational tetrahedral order, and (c) local structure index. Red dashed lines indicate order parameters for bulk TIP3P water in simulations of the same parameterization as RM production systems.

The time evolution of the average number of AOTs per RM is

$$\langle N_{\text{AOT}}^{\text{RM}} \rangle = \frac{1}{N_{\text{RM}}} \sum_{i=1}^{N_{\text{RM}}} N_{\text{AOT}_i}^{\text{RM}}(t), \quad (21)$$

where $\langle N_{\text{AOT}}^{\text{RM}} \rangle$ is the average number of AOTs per RM in the system shown in Fig. 9(a) alongside the functional fit derived from the master equation model. In the fitting process, we obtained the initial kinetic rate parameters *without* the RM collision-induced exchange term, k_{ex} , using an analytical solution of the master equation.⁷⁵ The initial exchange rate was set equal to the fusion rate: $k_{ex} = \bar{k}_+$. Based on these initial parameters, our new moment closure equations (including k_{ex}) were numerically solved according to Eqs. (14) and (15) using a least squares minimization method for the average RM size time series beyond 20 ns, corresponding to the time scale of RM fusion.

To test the robustness of these initial rate constants, all but the primary nucleation rate (k_n) constants were independently adjusted from 0.01 to 100 times their initial values prior to least squares optimization, which converged to the same solution. We applied a few constraints on the acceptable values of the kinetic parameters during optimization based on the small amount of kinetic information available and physical intuition. The nucleation, association, disassociation, fusion, fragmentation, and exchange rates were limited

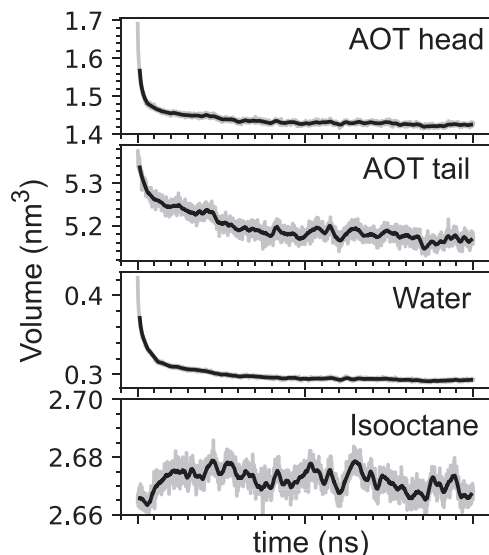


FIG. 8. Average Voronoi tessell volumes with shaded standard deviations of heavy atoms for AOT head groups, AOT tails, waters, and isooctane molecules averaged over 10 trajectories.

to $1 < k_n < 10^{15} \text{ M}^{-1} \text{ s}^{-1}$, $1 < k_+ < 10^{18} \text{ M}^{-1} \text{ s}^{-1}$, $0.1 < k_- < 10^{15} \text{ s}^{-1}$, $1 < \bar{k}_+ < 10^{10} \text{ M}^{-1} \text{ s}^{-1}$, $10^5 < \bar{k}_- < 10^{15} \text{ s}^{-1}$, and $10^7 < k_{ex} < 10^{19} \text{ M}^{-1} \text{ s}^{-1}$, respectively. The lower limit of the fragmentation rate, $\bar{k}_- = 10^5 \text{ s}^{-1}$, was based on the single observation of a fragmentation event on the time scale of our 10 400ns simulations.

During fitting, the fusion parameter (\bar{k}_+) was found to be 1000 times smaller than exchange rate (k_{ex}), corresponding to previous experimental studies³⁴ that estimated the order of this difference (σ) to be between 10^{-3} and 10^{-4} . The effect of this relation, $\bar{k}_+ = \sigma k_{ex}$, is demonstrated in Fig. 9(b). Our results show that setting $\sigma = 10^{-3}$ or 10^{-4} does not significantly influence the predictions of the model while if σ is very large, the predicted average sizes become large. This is reasonable as a larger σ implies that RMs fuse more frequently upon encounter. This suggests that there may be a large energy barrier which suppresses RM fusion during an encounter between RMs, thereby stabilizing the RM phase. The kinetic rates obtained from this numerical solution are

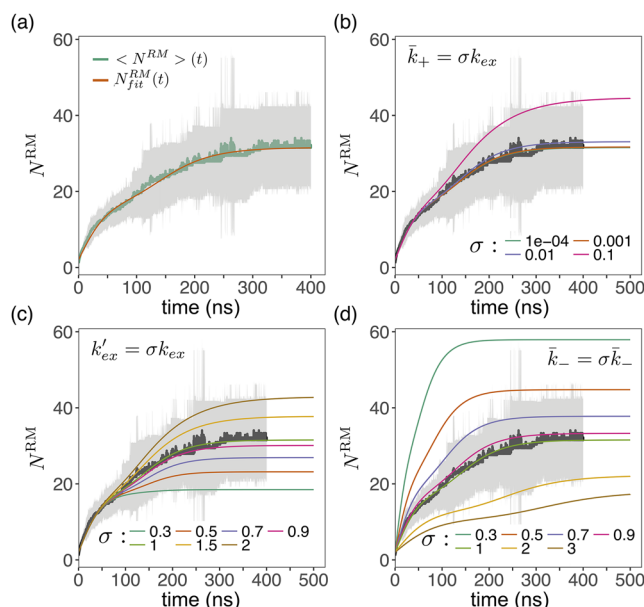


FIG. 9. (a) Average AOT aggregation number for RM clusters derived from ten MD trajectories (orange) and its standard deviation at each time (gray). The fitting line derived from the numerical solution of the moment equations defined by Eqs. (14) and (15) is shown for comparison. (b) Using the rate constant parameters, time evolution of the average size was derived from numerical solution exploring the effect of different magnitudes of fusion constants scaled to the exchange rate $\bar{k}_+ = \sigma k_{ex}$. Legend values show the scaling parameters of $\bar{k}_+ = \sigma k_{ex}$. The effect of varying scales of (c) exchange rate $k'_{ex} = \sigma k_{ex}$ and (d) fragmentation rate constants, $\bar{k}_- = \sigma \bar{k}_-$. The other kinetic rate parameters in (b)–(d) are those reported in Table I.

TABLE I. The RM kinetic rate constants derived from analyzing AOT size evolution derived from MD simulations using the numerical solution of the moment closure equations including the collision exchange process [Eqs. (13)–(15)].

Process	Rate constant
Primary nucleation k_n	$2.7 \times 10^5 \text{ M}^{-1} \text{ s}^{-1}$
Association k_+	$3.7 \times 10^9 \text{ M}^{-1} \text{ s}^{-1}$
Disassociation k_-	$2.3 \times 10^5 \text{ s}^{-1}$
Fusion \bar{k}_+	$k_{ex} \times 10^{-3} \text{ M}^{-1} \text{ s}^{-1}$
Fragmentation \bar{k}_-	$2.4 \times 10^6 \text{ s}^{-1}$
Exchange k_{ex}	$2.9 \times 10^{10} \text{ M}^{-1} \text{ s}^{-1}$

listed in Table I. These values have a precision on the order of 10 due to the standard deviation about the average RM size time series.

The exchange rate constant has been shown to be sensitive to system conditions,³⁴ reported to take values from 10^6 to $10^8 \text{ M}^{-1} \text{ s}^{-1}$ for water loadings between 10 and 30 in a range of conditions. Our estimated exchange rate is much faster than this range of values. As demonstrated in the past, the water loading and concentration of AOT and water can substantially change the exchange rate, rapidly increasing as the water loading decreases. As such, the very low water loading here is expected to produce a faster exchange rate. While our parameter optimization obtains unique solutions, the exact values of the resulting parameters are dependent on the specific $\langle N_{\text{AOT}}^{\text{RM}} \rangle$ time series employed. Thus, the standard error about $\langle N_{\text{AOT}}^{\text{RM}} \rangle$ may influence the kinetic rates determined by the model. In Fig. 9, we demonstrate the variations in $\langle N_{\text{AOT}}^{\text{RM}} \rangle$ when individual kinetic rates are independently varied.

We explored changing the kinetic rate parameters for collision, k_{ex} , and fragmentation, \bar{k}_- , to observe the impact on aggregation kinetics. Figures 9(c) and 9(d) show the effect of variation in these parameters leaving all other rate constants unchanged. The final average RM size between k_{ex} and \bar{k}_- converges to the same size if the factor between k_{ex} and \bar{k}_- is between 0 and 2. On the other hand, the time to reach the converged RM size, $N_{\text{AOT}}^{\text{RM}}(t) = N_{\text{AOT}}^{\text{RM}}(\infty)$, is sensitive to these rates. The increase in either exchange or fragmentation rate beyond a factor of two can make variations in the predicted RM size substantially larger. As shown in previous experiments,³⁴ such exchange rates can quickly change with variations in the system conditions, such as changes in the temperature or composition. These major changes to the exchange rate can explain why the RM phase is observed in a restricted temperature range. To form stable RMs, interactions among RMs must induce an exchange rate slower than the fragmentation rate, leading to the formation of moderately sized RMs. Our model quantifies how these rate constants determine the size of formed aggregates. In the future, as additional experimental exchange rates are determined for particular system conditions given the knowledge of the average RM size time series, our kinetic model may be used to accurately predict other elementary kinetic rates that might otherwise be difficult or impossible to determine. The form of our kinetic model might potentially be applied to related physical

phenomena, such as the normal surfactant micelle or lipid domain assembly.

CONCLUSIONS

We performed molecular dynamics simulations of AOT reverse micelle (RM) self-assembly at water loading $w_0 = 5$ and analyzed the dynamics and structure of RMs as a function of RM size, number of components, and time. Using ten independent replicate simulations initiated from random mixtures, we characterized (1) the mechanism of RM primary nucleation, (2) the structure of RMs during the RM fusion process, and (3) inferred the elementary rates describing RM nucleation, monomer association and disassociation, RM fusion and fragmentation, and the exchange of AOTs between RMs. We characterized the nascent dynamics that establish water loading on RMs within 1 ns by comparison to a diffusion-adsorption model which reproduces the distribution of molecular aggregates during this mechanism. The characteristic time scale of initial RM formation was found to be 20 ns in agreement with prior reports.⁶⁴ At longer times, the coalescence of small RMs occurs from 20 to 100 ns, followed by a slower fusion of large RMs until the average RM size reaches equilibrium. In the first 20 ns, the volume of individual molecular components was observed to rapidly decrease when forming RM aggregates. From 20 to 200 ns, the volume of the RM aggregates was observed to gradually converge. During this time, water in the core of RMs establishes the orientationally ordered structure unique from bulk-phase water. Beyond this time scale, no significant structural changes in RM aggregates were observed. However, our simulations do not appear to reach equilibrium as the observed RM size distributions do not achieve the narrow distribution that is expected based on thermodynamic arguments.

To describe the mechanics of RM collision-induced exchange on a longer time scale, we developed a novel moment-closed equation from a master equation describing RM growth including a collision-induced exchange process. The model shows the effects of molecular exchange upon RM collisions on average RM size. Changes in average RM size can be caused by slight changes in the salt, temperature, or AOT concentration, and substantial variation of average RM size may occur as a result of changes in these conditions. Using our proposed master equation model, we demonstrate that RM formation is only possible in a restricted range of conditions. Previous reports indicate that a change of a few degrees in temperature can increase the exchange rate by a factor of two.³⁴ Small-angle neutron scattering experiments at a water loading of 100 (large RM sizes) showed that the RM phase can transition to a phase separated state at slightly heightened temperatures while smaller RMs formed at water loadings of 30 did not undergo a phase transition over a 70° temperature range.⁹⁹ Increases in the exchange rate over those observed in this work would be necessary to support a transition to a phase separated state, which would likely require larger-scale simulations.^{100,101}

These simulations were performed at a very high concentration of AOT and water due to computational limitations on the system size. As our simulations were performed at

compositions known to form RMs, we believe finite size effects are minimal. Deviations from the past measurements of the exchange rate reflect the differing concentrations of AOT and water employed. In the future, the interplay of RM stability, size, and exchange rates might be explored at more dilute concentrations with larger simulation sizes on advanced hardware.

We performed 10 400ns simulations to apply our kinetic method to investigate the effect of each microscopic process. In this nanosecond scale, the average RM size converged to 31 ± 9 , within the error of the experimentally determined average size in *n*-octane,¹⁰² 30, and the previously reported 35 ± 8.5 reported in an equivalent MD study.⁶⁴ Hence, at the super- μ s time scale, the average RM size is not expected to increase while inter-micelle exchange is expected to decrease the dispersity of RM sizes in solution. Much longer simulations would be necessary to obtain a size distribution with the narrow polydispersity expected at equilibrium.

It should be noted that the AOT RM system can have slower exchange rates compared to most RM-forming surfactants,³⁴ implying that the time required for self-assembly in other RM systems is substantially shorter. Because AOT RMs are kinetically more stable than other RM systems, careful investigation of the self-assembly of other surfactant micelle systems will be essential in understanding the role of co-surfactant and the general mechanism of RM self-assembly. Our master equation approach provides a general framework through which to investigate the mechanism of RM formation and the role of co-surfactant RM mixtures applicable to data derived from simulation and experiment.

SUPPLEMENTARY MATERIAL

See [supplementary material](#) for (1) the visualization of Voronoi tessellation of an RM, (2) p-values of Kolmogorov-Smirnov, Wilcoxon signed rank, Wald-Wolfowitz tests between diffusion-adsorption and molecular dynamics simulations aggregate size distributions during initial RM formation, (3) the formulation of the original master equation model of Knowles and co-workers, (4) the steady state solution of the master equation model presented here, (5) the early time solution for the master equation model, and (6) the number of water molecules per RM averaged over all trajectories.

ACKNOWLEDGMENTS

This work was made possible through the generous support of the National Science Foundation (Grant No. CHE-1362524). G.A.P. and J.E.S. thank the NSF GRFP for support (Grant No. DGE-1247312).

¹D.-H. Zhang, Z. Guo, X.-Y. Dong, and Y. Sun, *Biotechnol. Prog.* **23**, 108 (2007).

²T. Hino, Y. Kawashima, and S. Shimabayashi, *Adv. Drug Delivery Rev.* **45**, 27 (2000).

³H. Okochi and M. Nakano, *Adv. Drug Delivery Rev.* **45**, 5 (2000).

⁴S. Higashi and T. Setoguchi, *Adv. Drug Delivery Rev.* **45**, 57 (2000).

⁵Y. Nishii, T. Kinugasa, S. Nii, and K. Takahashi, *J. Membr. Sci.* **195**, 11 (2002).

⁶N. V. Nucci, K. G. Valentine, and A. J. Wand, *J. Magn. Reson.* **241**, 137 (2014).

⁷I. Dodevski, N. V. Nucci, K. G. Valentine, G. K. Sidhu, E. S. O'Brien, A. Pardi, and A. J. Wand, *J. Am. Chem. Soc.* **136**, 3465 (2014).

⁸H.-F. Eicke and H. Christen, *Helv. Chim. Acta* **61**, 2258 (1978).

⁹W. Wong, J. Thomas, and M. Gratzel, *J. Am. Chem. Soc.* **98**, 6970 (1976).

¹⁰T. K. Jain and A. Maitra, *Colloids Surf.* **36**, 87 (1989).

¹¹T. K. Jain, M. Varshney, and A. Maitra, *J. Phys. Chem.* **93**, 7409 (1989).

¹²B. Valeur and E. Keh, *J. Phys. Chem.* **83**, 3305 (1979).

¹³M. Belletete, M. Lachapelle, and G. Durocher, *J. Chem. Phys.* **94**, 7642 (1990).

¹⁴H. Hauser, G. Haering, A. Pande, and P. L. Luisi, *J. Phys. Chem.* **93**, 7869 (1989).

¹⁵A. Maitra, *J. Phys. Chem.* **88**, 5122 (1984).

¹⁶H.-F. Eicke and P. Kvita, "Reverse micelles and aqueous microphases," in *Reverse Micelles, Reverse Micelles* (Springer Science + Business Media, 1984), pp. 21–35.

¹⁷M. Zulauf and H. F. Eicke, *J. Phys. Chem.* **83**, 480 (1979).

¹⁸F. Menger, J. Donohue, and R. Williams, *J. Am. Chem. Soc.* **95**, 286 (1973).

¹⁹F. Menger and G. Saito, *J. Am. Chem. Soc.* **100**, 4376 (1978).

²⁰M. Wong, M. Grätzel, and J. Thomas, *Chem. Phys. Lett.* **30**, 329 (1975).

²¹L. J. Magid, K. Kon-No, and C. Martin, *J. Colloid Interface Sci.* **83**, 307 (1981).

²²M. A. Rodgers, *J. Phys. Chem.* **85**, 3372 (1981).

²³A. Maitra and T. K. Jain, *Colloids Surf.* **28**, 19 (1987).

²⁴F. Tokiwa and T. Isemura, *Bull. Chem. Soc. Jpn.* **35**, 1737 (1962).

²⁵N. Pilpel, *Trans. Faraday Soc.* **56**, 893 (1960).

²⁶N. Pilpel, *Trans. Faraday Soc.* **57**, 1426 (1961).

²⁷A. Maitra, C. Mathew, and M. Varshney, *J. Phys. Chem.* **94**, 5290 (1990).

²⁸S. Bhattacharya, J. Stokes, M. Kim, and J. Huang, *Phys. Rev. Lett.* **55**, 1884 (1985).

²⁹G. S. Grest, I. Webman, S. Safran, and A. Bug, *Phys. Rev. A* **33**, 2842 (1986).

³⁰C. Mathew, P. K. Patanjali, A. Nabi, and A. Maitra, *Colloids Surf.* **30**, 253 (1988).

³¹M. D'Angelo, D. Fioretto, G. Onori, L. Palmieri, and A. Santucci, *Colloid Polym. Sci.* **273**, 899 (1995).

³²Y. Feldman, N. Kozlovich, I. Nir, N. Garti, V. Archipov, Z. Idiyatullin, Y. Zuev, and V. Fedotov, *J. Phys. Chem.* **100**, 3745 (1996).

³³M. Giustini, G. Palazzo, G. Colafemmina, M. Della Monica, M. Giomini, and A. Ceglie, *J. Phys. Chem.* **100**, 3190 (1996).

³⁴P. D. I. Fletcher, A. M. Howe, and B. H. Robinson, *J. Chem. Soc., Faraday Trans. 1* **83**, 985 (1987).

³⁵B. H. Robinson, D. C. Steytler, and R. D. Tack, *J. Chem. Soc., Faraday Trans. 1* **75**, 481 (1979).

³⁶S. Atik and J. Thomas, *J. Am. Chem. Soc.* **103**, 4279 (1981).

³⁷S. Atik and J. Thomas, *Chem. Phys. Lett.* **79**, 351 (1981).

³⁸S. Atik and J. Thomas, *J. Phys. Chem.* **85**, 3921 (1981).

³⁹J. Tian and A. E. Garcia, *Biophys. J.* **96**, L57 (2009).

⁴⁰J. Tian and A. E. Garcia, *J. Chem. Phys.* **134**, 225101 (2011).

⁴¹A. V. Martinez, E. Małolepsza, L. Domínguez, Q. Lu, and J. E. Straub, *J. Phys. Chem. B* **119**, 9084 (2015).

⁴²A. V. Martinez, E. Małolepsza, E. Rivera, Q. Lu, and J. E. Straub, *J. Chem. Phys.* **141**, 22D530 (2014).

⁴³G. Eskici and P. H. Axelsen, *J. Am. Chem. Soc.* **139**, 9566 (2017).

⁴⁴S. Abel, F. Sterpone, S. Bandyopadhyay, and M. Marchi, *J. Phys. Chem. B* **108**, 19458 (2004).

⁴⁵A. V. Nevidimov and V. F. Razumov, *Mol. Phys.* **107**, 2169 (2009).

⁴⁶A. V. Nevidimov and V. F. Razumov, *Colloid J.* **75**, 191 (2013).

⁴⁷J. Faeder and B. M. Ladanyi, *J. Phys. Chem. B* **104**, 1033 (2000).

⁴⁸J. Faeder and B. M. Ladanyi, *J. Phys. Chem. B* **105**, 11148 (2001).

⁴⁹J. Faeder, M. V. Albert, and B. M. Ladanyi, *Langmuir* **19**, 2514 (2003).

⁵⁰J. Faeder and B. M. Ladanyi, *J. Phys. Chem. B* **109**, 6732 (2005).

⁵¹J. Chowdhary and B. M. Ladanyi, *J. Phys. Chem. B* **113**, 15029 (2009).

⁵²J. Chowdhary and B. M. Ladanyi, *J. Phys. Chem. A* **115**, 6306 (2011).

⁵³G. Eskici and P. H. Axelsen, *J. Phys. Chem. B* **120**, 11337 (2016).

⁵⁴G. Eskici and P. H. Axelsen, *Langmuir* **34**, 2522 (2018).

⁵⁵A. Khoshnood and A. Firoozabadi, *Langmuir* **31**, 5982 (2015).

⁵⁶E. Duboué-Dijon and D. Laage, *J. Phys. Chem. B* **119**, 8406 (2015).

⁵⁷P.-L. Chau and A. Hardwick, *Mol. Phys.* **93**, 511 (1998).

⁵⁸J. R. Errington and P. G. Debenedetti, *Nature* **409**, 318 (2001).

⁵⁹E. Shiratani and M. Sasai, *J. Chem. Phys.* **104**, 7671 (1996).

- ⁶⁰G. Ruocco, M. Sampoli, and R. Vallauri, *J. Chem. Phys.* **96**, 6167 (1992).
- ⁶¹M. Muthukumar and R. Nossal, *J. Chem. Phys.* **139**, 121928 (2013).
- ⁶²A. Gardner, V. R. Vasquez, A. Clifton, and O. A. Graeve, *Fluid Phase Equilib.* **262**, 264 (2007).
- ⁶³V. R. Vasquez, B. C. Williams, and O. A. Graeve, *J. Phys. Chem. B* **115**, 2979 (2011).
- ⁶⁴M. Marchi and S. Abel, *J. Phys. Chem. Lett.* **6**, 170 (2015).
- ⁶⁵H.-F. Eicke, "Surfactants in nonpolar solvents," in *Topics in Current Chemistry* (Springer Science + Business Media), pp. 85–145.
- ⁶⁶P. Jones, E. Wyn-Jones, and G. J. Tiddy, *J. Chem. Soc., Faraday Trans. 1* **83**, 2735 (1987).
- ⁶⁷F. da Costa, *Mathematics of Energy and Climate Change* (Springer, 2015), pp. 83–162.
- ⁶⁸A. K. Shchekin, I. A. Babintsev, and L. T. Adzhemyan, *J. Chem. Phys.* **145**, 174105 (2016).
- ⁶⁹M. D. Hatlee and J. J. Kozak, *J. Chem. Phys.* **72**, 4358 (1980).
- ⁷⁰M. D. Hatlee and J. J. Kozak, *J. Chem. Phys.* **74**, 1098 (1981).
- ⁷¹S. I. Cohen, M. Vendruscolo, M. E. Welland, C. M. Dobson, E. M. Terentjev, and T. P. Knowles, *J. Chem. Phys.* **135**, 065105 (2011).
- ⁷²S. I. Cohen, M. Vendruscolo, C. M. Dobson, and T. P. Knowles, *J. Chem. Phys.* **135**, 065106 (2011).
- ⁷³S. I. Cohen, M. Vendruscolo, C. M. Dobson, and T. P. Knowles, *J. Chem. Phys.* **135**, 065107 (2011).
- ⁷⁴S. I. Cohen, S. Linse, L. M. Luheshi, E. Hellstrand, D. A. White, L. Rajah, D. E. Otzen, M. Vendruscolo, C. M. Dobson, and T. P. Knowles, *Proc. Natl. Acad. Sci. U. S. A.* **110**, 9758 (2013).
- ⁷⁵T. C. Michaels and T. P. Knowles, *J. Chem. Phys.* **140**, 214904 (2014).
- ⁷⁶G. N. Clark, G. L. Hura, J. Teixeira, A. K. Soper, and T. Head-Gordon, *Proc. Natl. Acad. Sci. U. S. A.* **107**, 14003 (2010).
- ⁷⁷P. J. Steinhardt, D. R. Nelson, and M. Ronchetti, *Phys. Rev. B* **28**, 784 (1983).
- ⁷⁸Y. Wang, S. Teitel, and C. Dellago, *J. Chem. Phys.* **122**, 214722 (2005).
- ⁷⁹W. Lechner and C. Dellago, *J. Chem. Phys.* **129**, 114707 (2008).
- ⁸⁰S. Auer and D. Frenkel, *J. Chem. Phys.* **120**, 3015 (2004).
- ⁸¹R Core Team, R: A Language and Environment for Statistical Computing, R Foundation for Statistical Computing, Vienna, Austria, 2017.
- ⁸²R. Ihaka and R. Gentleman, *J. Comput. Graph. Stat.* **5**, 299 (1996).
- ⁸³K. Soetaert, T. Petzoldt, and R. W. Setzer, *J. Stat. Software* **33**, 1 (2010).
- ⁸⁴M. L. Delignette-Muller and C. Dutang, *J. Stat. Software* **64**, 1 (2015).
- ⁸⁵D. Eddelbuettel and R. François, *J. Stat. Software* **40**, 1 (2011).
- ⁸⁶D. Eddelbuettel, *Seamless R and C++ Integration with Rcpp* (Springer, New York, 2013), ISBN: 978-1-4614-6867-7.
- ⁸⁷H. Wickham, *ggplot2: Elegant Graphics for Data Analysis* (Springer-Verlag New York, 2009).
- ⁸⁸A. Signorell *et al.*, DescTools: Tools for Descriptive Statistics, r package version 0.99.21, 2017.
- ⁸⁹B. Tamamushi and N. Watanabe, *Colloid Polym. Sci.* **258**, 174 (1980).
- ⁹⁰P. Bjelkmar, P. Larsson, M. A. Cuendet, B. Hess, and E. Lindahl, *J. Chem. Theory Comput.* **6**, 459 (2010).
- ⁹¹D. Van Der Spoel, E. Lindahl, B. Hess, G. Groenhof, A. E. Mark, and H. J. Berendsen, *J. Comput. Chem.* **26**, 1701 (2005).
- ⁹²F. Sterpone, M. Ceccarelli, and M. Marchi, *J. Phys. Chem. B* **107**, 11208 (2003).
- ⁹³H. J. Berendsen, D. van der Spoel, and R. van Drunen, *Comput. Phys. Commun.* **91**, 43 (1995).
- ⁹⁴S. Pall, M. J. Abraham, C. Kutzner, B. Hess, and E. Lindahl, in *International Conference on Exascale Applications and Software* (Springer, 2014), pp. 3–27.
- ⁹⁵M. J. Abraham, T. Murtola, R. Schulz, S. Páll, J. C. Smith, B. Hess, and E. Lindahl, *SoftwareX* **1**, 19 (2015).
- ⁹⁶B. Hess, H. Bekker, H. J. Berendsen, J. G. Fraaije *et al.*, *J. Comput. Chem.* **18**, 1463 (1997).
- ⁹⁷B. Hess, *J. Chem. Theory Comput.* **4**, 116 (2008).
- ⁹⁸U. Essmann, L. Perera, M. L. Berkowitz, T. Darden, H. Lee, and L. G. Pedersen, *J. Chem. Phys.* **103**, 8577 (1995).
- ⁹⁹B. H. Robinson, C. Toprakcioglu, J. C. Dore, and P. Chieux, *J. Chem. Soc., Faraday Trans. 1* **80**, 13 (1984).
- ¹⁰⁰G. A. Pantelopulos, T. Nagai, A. Bandara, A. Panahi, and J. E. Straub, *J. Chem. Phys.* **147**, 095101 (2017).
- ¹⁰¹J. Huang and G. W. Feigenson, *Biophys. J.* **65**, 1788 (1993).
- ¹⁰²T. K. De and A. Maitra, *Adv. Colloid Interface Sci.* **59**, 95 (1995).